Article

Colloidal Properties of Aqueous Suspensions of Acid-Treated, Multi-Walled Carbon Nanotubes

Billy Smith, Kevin Wepasnick, K. E. Schrote, A. R. Bertele, William P. Ball, Charles O'Melia, and D. Howard Fairbrother

Environ. Sci. Technol., **2009**, 43 (3), 819-825 • DOI: 10.1021/es802011e • Publication Date (Web): 29 December 2008

Environ. Sci. Technol. **2009,** *43,* 819–825

Colloidal Properties of Aqueous Suspensions of Acid-Treated, Multi-Walled Carbon Nanotubes

BILLY SMITH,[†] KEVIN WEPASNICK,[†] K. E. SCHROTE,[§] A. R. BERTELE,[§] WILLIAM P. BALL,[∥] CHARLES O'MELIA,[∥] AND D. HOWARD FAIRBROTHER*[,†,‡]

Department of Chemistry, The Johns Hopkins University, Baltimore, Maryland 21218, Department of Materials Science and Engineering, The Johns Hopkins University, Baltimore, Maryland 21218, Department of Chemistry, College of Notre Dame of Maryland, Baltimore, Maryland., Department of Geography and Environmental Engineering, The Johns Hopkins University, Baltimore, Maryland 21218 July, 2008

Received July 19, 2008. Revised manuscript received October 13, 2008. Accepted October 23, 2008.

Grafting oxygen-containing functional groups onto carbon nanotubes (CNTs) by acid treatment improves their dispersion in aqueous solutions, but there is a lack of quantitative information on the colloidal properties of oxidized CNTs. We have studied the influence that pH and electrolytes have in determining the colloidal stability of oxidized multiwalled carbon nanotubes (O-MWCNTs), prepared by refluxing pristine MWCNTs in nitric acid. The acid-treated MWCNTs contained oxygen predominantly in the form of carboxyl groups. Colloidal suspensions of O-MWCNTs were prepared by low-power sonication and contained negatively charged, individual MWCNTs with an average length of ~650 nm. Time-resolved dynamic light scattering revealed that the aggregation rate of O-MWCNTs exhibited both reaction and mass-transport limited regimes in the presence of different electrolytes and as a function of pH. Particle stability profiles constructed from aggregation rate data allowed for the determination of critical coagulation concentrations (CCC), a metric of colloidal stability. The CCC values of O-MWCNTs varied with counterion concentration and valence in a manner consistent with DLVO theory. Potentiometric measurements of surface charge correlated well with the observed pH-dependent variations in the O-MWCNT's colloidal stability. Electrophoretic mobility was also a diagnostic of particle stability, but only in neutral and acidic conditions.

Introduction

Carbon nanotubes (CNTs) are hexagonal arrays of carbon atoms rolled into long (μm scale), thin (nm scale), hollow cylinders (*1*). Their unique structure and chemical composition give rise to many highly desirable properties, including low density, high tensile strength, high conductivity, and high surface area to volume ratios (*2, 3*). Consequently, the number of potential commercial applications incorporating CNTs is enormous, providing the impetus for dramatic increases in their annual production rates: Bayer anticipates production rates of 200 tons/yr by 2009, and 3,000 tons/yr by 2012 (*4*).

Many CNT applications (e.g., as components of drug delivery agents, composite materials) require CNT suspensions that remain stable in polar mediums such as water or polymeric resins (*5, 6*). Due to strongly attractive van der Waals forces between the hydrophobic graphene surfaces, pristine CNTs minimize their surface free energy by forming settleable aggregates in solution. To prepare uniform, well-dispersed mixtures, the CNTs' exterior surface must be modified. One popular surface modification technique involves grafting hydrophilic oxygen-containing functional groups into the exterior graphene sheet by using strong oxidizing agents (e.g., HNO_3, HNO_3/H_2SO_4, O_3, $KMnO_4$ or H_2O_2) (*7*−*9*). During these oxidative treatments, oxygen-containing functional groups form at the CNT's exposed surfaces, preferentially at open ends and defect sites (*10*).

The introduction of surface oxides onto CNTs is not always intentional. In purification processes, surface oxidation accompanies the use of oxidants that are frequently employed to remove amorphous carbon and metallic impurities from freshly synthesized CNTs (*9, 11*−*13*). In the atmosphere, unintentional oxidation can occur when CNTs are exposed to oxidizing agents such as ozone and hydroxyl radicals (*14*). Incidental oxidation in aquatic environments may occur as a result of surface water photolysis and strongly oxidizing water treatment processes (e.g., ozonolysis) (*15*).

The demand for dispersible CNTs and the potential for incidental oxidation of the pristine nanomaterial will lead to increasing quantities of surface-oxidized CNTs in aquatic environments (*16, 17*), where oxygen-containing functional groups will influence the CNTs' interactions with other dissolved species. For example, the sorption of hydrophobic organic chemicals from water has recently been shown to decrease significantly in the presence of surface oxides (*18*), whereas the sorption of metal contaminants increases (*17, 19, 20*). Since the human and ecological impact of engineered nanomaterials in aquatic media will be intimately dependent upon their sorption properties and colloidal stability (*16, 21, 22*), surface-oxidized CNTs are of particular environmental interest.

To better understand the influence of solution chemistry on the behavior of nanoparticles, several recent studies have used time-resolved dynamic light scattering (TRDLS) to measure the aggregation kinetics of various colloidal nanoparticles (fullerenes, hematite, and zerovalent iron) (*23*−*29*). By measuring the functional dependence of the aggregation rates on electrolyte concentration (aggregation profiles), critical coagulation concentrations (CCC) were determined under different aquatic conditions. Results from these studies have demonstrated that the behavior of nanoparticles follows the qualitative predictions of Derjaguin−Landau−Verwey−Overbeek (DLVO) theory (*30, 31*) in regard to the effect of counterion concentration and valence.

Although CNTs are an important class of engineered nanomaterials, few studies have quantitatively investigated the colloidal properties of acid-treated, surface-oxidized CNTs. Chen et al. used light scattering to show that single-walled nanotubes refluxed in HNO_3 and then sonicated in HNO_3/H_2SO_4 remained stable at neutral pH over a two week period (*32*). Shieh et al. employed UV−visible spectrophotometry (UV−vis) to show that acid-treated MWCNTs were unstable at pH 0 but increased in aquatic stability between pH 4 and 10, an effect ascribed to the protonation/deprotonation of carboxylic acid groups (*33*). The oxidation of

* Corresponding author e-mail: howardf@jhu.edu.
[†] Department of Chemistry, The Johns Hopkins University.
[§] Department of Chemistry, College of Notre Dame of Maryland.
[∥] Department of Geography and Environmental Engineering, The Johns Hopkins University.
[‡] Department of Materials Science and Engineering, The Johns Hopkins University.

10.1021/es802011e CCC: $40.75
Published on Web 12/29/2008

MWCNTs by HNO_3 or HNO_3/H_2SO_4 has also been investigated by Osswald et al. who observed the formation of negatively charged particles that exhibited an electrophoretic mobility of ~ -4 μm s^{-1} cm V^{-1} at neutral pH (*34*). Sano et al. used UV−vis to show that the aquatic stability of acid-treated single-walled carbon nanotubes in different electrolytes was in good agreement with the Schulze−Hardy rule (*35*). By contrast, Giordano et al. have suggested that the rodlike morphology of CNTs means that their colloidal behavior should not follow classical DLVO theory (*36*).

In this study, the effect of solution chemistry on the colloidal properties of a surface-oxidized MWCNT has been measured with TRDLS and coupled with detailed materials characterization. Nitric acid was selected as the oxidant due to its widespread use in functionalizing and purifying CNTs (*12, 37*). MWCNTs were selected because they are currently being produced at higher rates than SWCNTs (*38*) and are therefore more likely to enter aquatic environments in larger quantities.

Experimental Section

Preparation of Oxidized MWCNTs (O-MWCNTs). Pristine MWCNTs were purchased from NanoLab (outer diameter 15 ± 5 nm, length 5−20 μm). As prepared by the manufacturer, MWCNTs initially contained 15% metal impurities (Fe or Ni) by weight, according to TGA analysis. These metal impurities are reportedly from the catalysts used to grow the MWCNT. To remove the metal catalyst, the MWCNTs were treated with a combination of HF/HCl. TGA experiments after treatment showed the metal content was reduced to <5%.

O-MWCNTs were prepared by refluxing 100 mg of pristine MWCNTs in a 250 mL solution of 50% w/w HNO_3. Prior to refluxing, the MWCNT-HNO_3 mixture was sonicated (Branson 1510, operating at 70 W) for 1 h to break up large aggregates and help disperse the nanomaterials. After sonication, the MWCNT-HNO_3 mixture was refluxed at 140 °C for 1.5 h while stirring vigorously.

After oxidation, byproducts were removed from the HNO_3-MWCNT mixture by repeatedly centrifuging (10 min, 4000 rpm; Powerspin LX, Unico), decanting and washing until the resistivity of the supernatant was greater than 0.5 MΩ and the pH was ~5. O-MWCNTs were then dried overnight in an oven at 100 °C. Once dry, the O-MWCNTs were pulverized in a ball-mill (MM200, Retsch) for 15 min.

Surface Characterization of O-MWCNTs. The surface composition of O-MWCNTs was determined using X-ray photoelectron spectroscopy (XPS), PHI 5400 system. The distribution of oxygen-containing functional groups on the O-MWCNT surface was quantified using vapor-phase chemical derivatization in conjunction with XPS. In brief, trifluoracetic anhydride, trifluoroethyl hydrazine, and trifluoroethanol were used to assay the concentration of surface-bound hydroxyl, carbonyl, or carboxylic acid groups as described elsewhere (*39, 40*).

Preparation of Colloidal O-MWCNTs. Stock solutions of colloidal O-MWCNTs were created by sonicating a known mass (<600 μg) of O-MWCNTs in 200 mL of Milli-Q water for ~20 h. After sonication, the solution pH was adjusted: pH 3 (~200 μL/1 M HCl), pH 4 (20 μL/1 M CH_3COOH/$NaCH_3COO$), pH 6 (100 μL/1 M CH_3COOH/$NaCH_3COO$), pH 8 (200 μL/0.1 M $NaHCO_3/Na_2CO_3$), or pH 10 (~20 μL/1 M NaOH). The majority of experiments were carried out at pH 6. Control experiments were performed to probe the influence of the acetate buffer on particle stability; these results are described in Figure S1 in the Supporting Information. The mixture was then sonicated for an additional hour. Any large contaminant particles (such as dust, glass etched during sonication, and some larger CNT bundles (<0.2% by mass) were removed at this stage by centrifugation. The pH was then readjusted by adding <200 μL aliquots of 0.01−0.1 M NaOH/HCl as needed. By using UV−vis to analyze a known mass of O-MWCNTs dispersed into solution, we have determined that the extinction coefficient of O-MWCNT particles at 500 nm was ~41.4 mL mg^{-1} cm^{-1}, independent of oxidative treatment. A similar value (39.9 mL mg^{-1} cm^{-1}) was also obtained by Li et al. (*41*) for dispersed, acid-washed MWCNTs.

Details of the atomic force microscopy (AFM), electrophoretic mobility, and surface charge measurements used to further characterize the O-MWCNTs can be found in the Supporting Information.

Dynamic Light Scattering (DLS) Measurements. The effective particle size of O-MWCNTs in solution was measured using DLS (Brookhaven Instruments, using an argon ion laser (488 nm) operating at 175 mW, aperture size 200 μm). MWCNTs are somewhat flexible, rod-like particles with high aspect ratios, but there is no analytic expression that can describe the orientational dependence on the intraparticle interactions for rod-like particles and consequently the DLVO theory for CNTs. Consequently, we have chosen to use the Stoke's−Einstein equation for spherical particles to determine the effective hydrodynamic diameter of the O-MWCNTs. For the purpose of developing comparative quantitative measures, we have also fit the aggregation kinetics on the basis of mathematical models developed to describe the coagulation of monodispersed spherical particles (*23, 25, 27, 42*).

In each aggregation experiment, separate aliquots containing O-MWCNTs (from the stock solution), milli-Q water, and electrolyte (4 M NaCl, 2 M Na_2SO_4, and 0.04 M $MgCl_2$ and 0.04 M $CaCl_2$) were prepared. Each aliquot was maintained at the same pH. Prior to aggregation, the effective intensity averaged hydrodynamic diameter (D_h) of the O-MWCNTs was determined. These experiments were initiated by mixing the aliquot of milli-Q water with the stock solution containing the O-MWCNT suspension in a 1-dram vial. The mixture was then vortexed for approximately 1 s, inserted into the decaline-quartz vat of the light scattering chamber, and thermally equilibrated at 25 °C for 1 min. The particle size (D_h ($t = 0$)) was determined by measuring the scattered light intensity for 15 s with a photodetector positioned at 90°. To accurately determine D_h ($t = 0$), 3−5 DLS measurements were performed; in each measurement, autocorrelations were fit with a second-order cumulant analysis.

After measuring the initial particle size, aggregation was initiated by adding the aliquot of electrolyte stock solution to the vial. In each series of aggregation experiments, the volume of O-MWCNT stock solution used was the same, while the volume of electrolyte solution and milli-Q water varied. Since the combined volume of O-MWCNT stock solution, milli-Q water, and electrolyte solution added always remained constant (2.2 mL), this experimental protocol ensured that the initial O-MWCNT particle density (N_0) remained constant in each aggregation experiment (see eq 2). Once the electrolyte had been added, the mixture was vortexed for approximately 1 s and promptly reinserted into the analysis chamber whereupon TRDLS measurements were initiated. To ensure that all data obtained were for particles aggregating under the influence of Brownian motion, the first TRDLS measurement taken after vortexing was ignored. All aggregation experiments were conducted in triplicate to verify experimental reproducibility and enable signal averaging.

Aggregation kinetics were measured by monitoring the time-dependent increase in D_h. Autocorrelation functions were analyzed every 15 s until D_h reached 400 nm or until 25 data points had been acquired. Measured values of $D_h \geq$ 800 nm (presumably due to residual dust particles or macroscopic aggregates entering the laser's field of view)

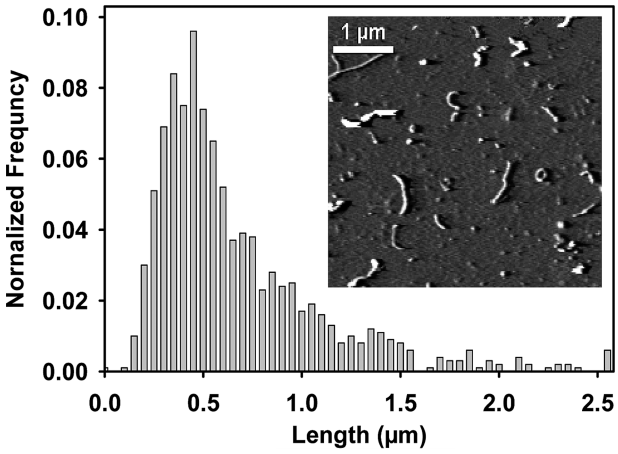

FIGURE 1. Frequency-normalized length distribution (measured with AFM and based on 1,000 measurements) of OMWCNTs sonicated for 20 h and flash dried on a Si substrate.

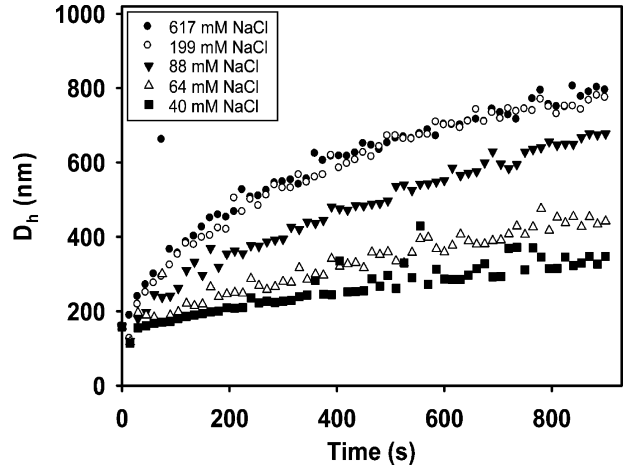

FIGURE 2. Aggregation profiles of OMWCNTs at various NaCl concentrations. Each profile was obtained at pH 6 and an O-MWCNT concentration of ~0.75 mg/L.

represented <1% of all the points acquired and were excluded from analysis.

Results and Discussion

Surface Characterization of O-MWCNTs. Upon oxidation with HNO_3, the XPS-measured surface oxygen concentration on the surface of the MWCNTs increases from 1.2% to 8.1% (Figure S2). No elements aside from carbon or oxygen were observed by XPS on pristine or O-MWCNTs. XPS results from chemical derivatized samples (Figure S3) revealed that pristine MWCNTs contain only trace concentrations (<1%) of hydroxyl, carbonyl, and carboxyl functional groups. After oxidation, the concentration of hydroxyl and carbonyl groups exhibited a modest increase while the carboxyl group concentration increased significantly. Carboxyl groups account for more than 50% of the surface oxygen atoms present on the O-MWCNT. To test whether the sonication process changed the material's chemical composition, the surface composition of an O-MWNCT was measured before and after sonication. XPS analysis revealed that sonication did not produce any measurable change in the surface oxygen concentration (<0.2%).

Characterization of Colloidal O-MWCNT Particles. The AFM images shown in Figure 1 as well as TEM images taken as part of our other studies reveal that the O-MWCNTs are best considered as rod-like structures that sometimes exhibit a mild degree of curvature. Occasionally, AFM images revealed the presence of "ring like" structures, likely a result of dehydration effects induced by drying. Similar effects have been observed in AFM studies of natural organic matter (*43*). In AFM images, individual O-MWCNTs were routinely observed as opposed to aggregates (Figure 1 insert), suggesting that oxidation followed by sonication results in predominantly individual MWCNTs.

Based on AFM measurements performed on 1,000 individual particles, colloidally dispersed MWCNTs exhibited a length distribution of $0.6 \pm 0.5\,\mu$m (Figure 1). Lengths ranged from 0.09 to 5.81 μm; 84% of the 1,000 measurements were below 1.00 μm. Compared to the manufacturer's stated length distribution for pristine MWCNTs (5−20 μm), sonicated O-MWCNTs were shorter and exhibit a narrower length distribution, consistent with previous studies on the effect of sonication (*44*).

DLS measurements indicated that the equivalent spherical hydrodynamic diameter (D_h) of the O-MWCNT colloids was 150 ± 40 nm (see Figure 2). In Milli-Q water at pH 6, the size distribution of O-MWCNT particulates remained unchanged over a period of several weeks. Changes in D_h during aggregation studies are therefore solely due to the effect of the added electrolytes.

Aggregation Studies. *Influence of the Electrolyte.* Using TRDLS, the aggregation kinetics of the O-MWCNTs were studied at pH 6 in the presence of various electrolytes: NaCl (30−900 mM), Na_2SO_4 (30−200 mM), $MgCl_2$ (1−8 mM), and $CaCl_2$ (0.7−6.2 mM). Irrespective of the electrolyte's chemical composition or concentration, a linear increase in D_h was observed during the initial stages of aggregation, between $D_h \sim 150-400$ nm (see Figure S4). During particle aggregation, the initial change in D_h is often characterized by a linear increase as a function of aggregation time (*23*−*28, 42*). This is a consequence of the fact that during these early times aggregation is dominated by bimolecular collisions involving individual particulates. As aggregation continues, the average aggregate size increases (leading to a decrease in mobility) while the overall particle concentration decreases. Consequently, the rate of change in D_h decreases (see Figure S4). Similar aggregation profiles have been observed in a number of other TR-DLS studies (*23*−*28, 42*).

The initial aggregation rate constant (k_a) was obtained by fitting the initial linear increase in D_h with time, using eq 1:

$$\left(\frac{dD_h}{dt}\right)_{t\to 0} = \Theta k_a N_0 \qquad (1)$$

where Θ is an instrumental constant that depends on the scattering angle and physical properties of the particles and N_0 is the initial number concentration of particles in solution (*23*−*27, 42*). Although D_h always increased linearly with time during the initial stages of aggregation, the magnitude of the initial aggregation rate was strongly dependent upon the solution conditions. Based on the precepts of DLVO theory, at sufficiently high electrolyte concentrations the electrostatic repulsion between negatively charged O-MWCNT particles (*23*−*29, 42*) is reduced to the point where there is no energy barrier to aggregation. Under these conditions, every collision results in an aggregation event, and the aggregation rate is diffusion-controlled. Experimentally this is observed by a rate of change in D_h that is invariant to further increases in electrolyte concentration. In Figure 2, this is clearly observed between the two highest NaCl concentrations (199 and 617 NaCl). Under these conditions of diffusion-limited aggregation, the initial rate of (dD_h/dt) is referred to as $(dD_h/dt)_{fast}$. At lower electrolyte concentrations, particles can only aggregate if they overcome the energetic barrier that is present due to the electrostatic repulsion between the particles. Under these conditions, the aggregation is said to be reaction-limited and is sensitive to the electrolyte concentration. For example,

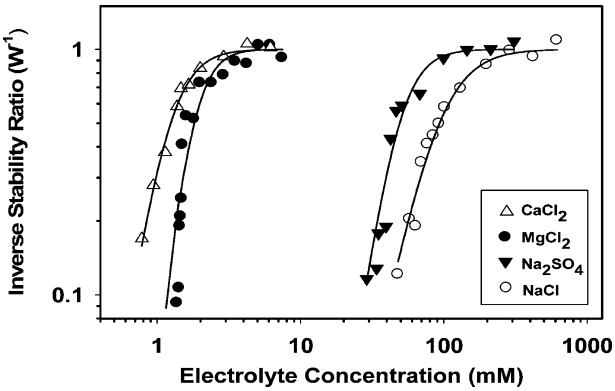

FIGURE 3. Influence of electrolyte composition on O-MWCNTs stability. Each stability profile was obtained at an O-MWCNT concentration of 0.75 mg/L at pH 6. Solid lines represent fits to eq 3. See text for details.

Figure 2 shows that when the NaCl concentration increased from 40 to 88 mM, the initial aggregation rate increased nearly 4-fold. These two regimes of aggregation have been reported in several recent aggregation studies (*23*−*27*) (*28*), and have also been interpreted on the basis of reaction and diffusion-limited kinetics. In the diffusion-limited regime, the initial rate of aggregation was obtained by averaging the 3 or 4 highest (dD_h/dt) values. Once this $(dD_h/dt)_{fast}$ value was determined, (dD_h/dt) values measured at lower electrolyte concentrations were normalized to $(dD_h/dt)_{fast}$. Eq 2 shows that since the initial particle concentration (N_0) was constant for a given set of aggregation studies, $(dD_h/dt)/(dD_h/dt)_{fast}$ is equal to $k_a/k_{a,fast}$.

The ratio of $k_a/k_{a,fast}$ is known as the inverse particle stability ratio (W^{1-}) or the aggregation attachment efficiency (α_A) (*25, 45*):

$$\frac{(dD_h/dt)_{t\to 0}}{(dD_h/dt)_{t\to 0}} = \frac{\Theta k_a N_0}{\Theta k_{a,fast} N_0} = \frac{k_a}{k_{a,fast}} = \frac{1}{W} = \alpha_A \qquad (2)$$

By plotting W^{1-} as a function of the electrolyte concentration, a stability profile is generated. Figure 3 shows the stability profiles of O-MWCNTs in the presence of NaCl, Na_2SO_4, $MgCl_2$, and $CaCl_2$. For each electrolyte, the average (dD_h/dt) values measured at high electrolyte concentration were the same, within experimental error (±8%). The critical coagulation concentration or CCC (an estimate of the minimum electrolyte concentration required for aggregation kinetics to be governed by mass-transport) was determined by fitting the stability profile using eq 3 (*27, 45*):

$$\frac{1}{W} = \frac{1}{1 + (CCC/[M^{n+}])^{\beta}} \qquad (3)$$

$[M^{n+}]$ is the counterion concentration (for negatively charged O-MWCNTs, $M^{n+} = Na^+$, Mg^{2+}, or Ca^{2+}), and β is $d\log(W^{1-})/d\log([M^{n+}])$ in the regime where $\log(W^{1-}) \propto \log([M^{n+}])$.

Analysis of the stability profiles shown in Figure 3 indicates that the CCC was 93 mM in the presence of NaCl, 98 mM for Na_2SO_4, 1.8 mM for $MgCl_2$, and 1.2 mM for $CaCl_2$. The similarity in the CCC values measured for NaCl and Na_2SO_4 points to the lack of influence that the anions (Cl^- and SO_4^{2-}) exert on the colloidal stability of the negatively charged O-MWCNT particles. For electrolytes that contain counterions of different valence, DLVO theory predicts that the CCC will be proportional to Z^{-6} for surfaces with high charge densities and Z^{-2} for surfaces with low charge densities (where Z is the counterion valence) (*25, 46*). Analysis of Figure 3 reveals that the ratio of the CCC between Na^+ ($Z = 1$) and Mg^{2+} or Ca^{2+} ($Z = 2$) is 52 and 78 respectively. These ratios for Mg^{2+} and Ca^{2+} are proportional to $Z^{-5.7}$ and $Z^{-6.3}$, very close to the empirical Schulze−Hardy rule and the DLVO theory prediction of Z^{-6} for surfaces with high charge densities (*30, 31*).

Results from our studies support the idea that the spherical particle approximation can be used to quantify the colloidal stability of O-MWCNTs. For example, the observed linear increase in D_h we observed for O-MWCNTs during the initial stages of aggregation follow the expected behavior of spherical particles (*23, 27, 28, 42*). Molecular dynamic simulations have shown that despite the influence of orientation on the interaction energy between rod-like structures, the distribution of cluster sizes during diffusion-limited aggregation follows the same general kinetic behavior observed for spherical particles (*47*). For spherical particles, this linear regime has been observed experimentally between D_h ($t = 0$) and ~1.4 D_h ($t = 0$), but for rod-like iron(III) hydroxide colloids, Brunner et al. found that this linear regime extended from D_h ($t = 0$) up to ~5 D_h ($t = 0$) (*48, 49*). For our O-MWCNTs, the linear increase in D_h was observed in the time regime between D_h ($t = 0$) and ~2.5 D_h ($t = 0$).

Our experimentally observed variation in initial (dD_h/dt) values for O-MWCNTs as a function of electrolyte concentration also produces both reaction and diffusion-limited aggregation regimes. The dependence of the CCC on Z^{-6} which is the analytical solution calculated for spherical particles from DLVO theory also supports the ability of the spherical particle approximation to describe the colloidal properties of O-MWCNTs (*30, 31*). This adherence to the qualitative precepts of DLVO theory for spherical particles is also consistent with the UV−vis data obtained by Sano et al. on acid-treated single-walled carbon nanotubes (*35*).

Influence of pH. Figure 4a shows a comparison of the aggregation kinetics for O-MWCNTs at pH 3, 6, and 10, each measured in the presence of 64 mM NaCl. Analysis of Figure 4a clearly shows that the colloidal stability of O-MWCNTs increases with increasing pH, consistent with previous UV−vis studies of acid-treated CNTs (*33*). The colloidal stability of the O-MWCNTs studied in this investigation is expressed quantitatively in Figure 4b where stability profiles obtained at pH 3, 4, 6, 8, and 10 are shown as a function of NaCl concentration. For all five pH values, both reaction and diffusion-limited aggregation regimes were observed. Particle stability profiles were all well described by eq 3; the calculated CCC values increased from 26, 46 to 93, 132, and 259 mM NaCl as the pH increased from 3, 4, 6, 8, and 10, respectively. Indeed, a linear correlation is observed between the CCC values and the pH (see Figure S5).

The role that pH plays in controlling the colloidal stability of O-MWCNTs is illustrated in Figure S6. In this experiment, three stable suspensions were initially created at the same MWCNT concentration (~4.2 mg O-MWCNT/L) but at different pH values (shown on each vial cap). The ionic strength in each vial was then increased to 64 mM with NaCl, and perikentic aggregation proceeded for 3.5 h. Figure S6 shows that after 3.5 h, large settleable aggregates had formed at pH 3, significantly smaller aggregates were observed at pH 6, and at pH 10 no visible aggregation was observed.

To better understand the influence of pH on CNT colloidal stability, the electrophoretic mobility (EM) of the O-MWCNT particles was measured as a function of pH, in the presence of 64 mM NaCl. Figure 5a shows that between pH 3 and 5 the EM decreases from −1.7 to −3.2 (10^{-8} m^2 V^{-1} s^{-1}). Taken in conjunction with the chemical derivatization data (Figure S3), these results support the idea that carboxyl groups play an important role in determining the colloidal stability of oxidized CNTs (*33*). Above pH 6 there is little or no change in the EM values, independent of the electrolyte concentration (see Figure S7). This behavior is analogous to previous EM measurements of oxidized carbon nanotubes (*50, 51*). However, a comparison of Figures 5a and 4b reveals that at

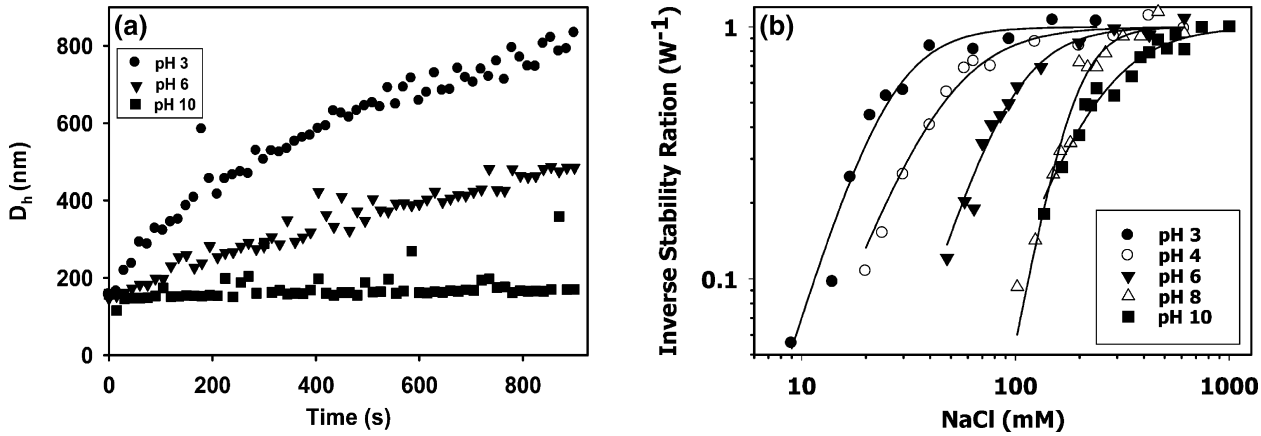

FIGURE 4. (a) Aggregation profiles of O-MWCNTs in the presence of 64 mM NaCl at pH 3, 6, and 10. (b) Stability profiles of O-MWCNTs at pH 3, 4, 6, 8, and 10. All experiments were conducted at an O-MWCNT concentration of ~0.75 mg/L.

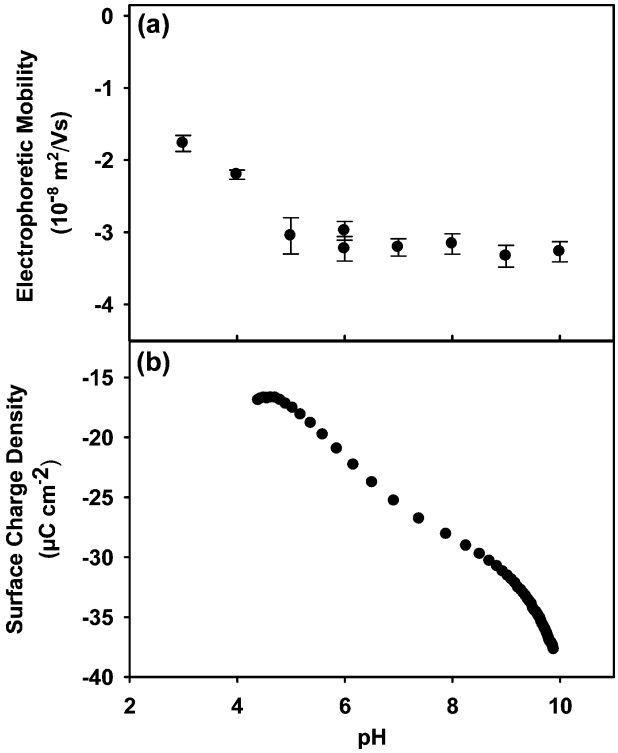

FIGURE 5. (a) Electrophoretic mobility and (b) surface charge density of O-MWCNTs as a function of pH in the presence of ~64 mM NaCl.

pH values >6 the lack of change in the EM values is consistent with the continued increase in the colloidal stability of the O-MWCNT particles. We hypothesize that this lack of correlation between the EM measurements and the CCC values is due to the fact that particle stability is not well reflected by the EM which is a measure of the surface charge density at the "zeta" plane, which is affected by a layer of water and counterions that remain with the particle as it moves in water under the influence of an electrostatic field. Our results from acid−base titration experiments, shown in Figure 5b are consistent with this hypothesis. In particular, these experiments show that the surface charge density increases monotonically with increasing pH, consistent with the greater colloidal stability of oxidized MWCNTs above pH 6 (compare Figures 4b and 5b).

The monotonic decrease in the surface charge observed for O-MWCNTs is similar to the behavior observed for other carbonaceous materials (e.g., activated carbon) (*52*). Since the surface charge continues to increase above pH 7, under conditions where all of the carboxylic acid groups should be deprotonated, other sources of surface charge must exist; possibilities include phenolic −OH groups or basic surface sites on CNTs. The detailed nature of such basic surface sites is unclear but may include the CNT graphene surface itself which could exhibit π basicity or pyrone-based oxygen functional groups (*53, 54*). The discrepancy between the variation in EM and surface charge as a function of pH has also been observed for other materials (e.g., silica) (*55*), highlighting the limitations of EM measurements to provide a metric of surface charge or particle stability.

Information obtained from this investigation can help to develop predictive models capable of describing the environmental fate and impact of surface-modified CNTs. For instance, our reported CCC values fall within the range of salinity conditions encountered in freshwater streams and estuaries. Thus, O-MWCNTs could be relatively stable against coagulation and sedimentation in these aquatic environments, depending upon the local solution conditions (pH, electrolyte composition/concentration, and other aspects of water quality, such as NOM concentration). Our data also indicate that although O-MWCNTs could be present as mobile colloids in freshwater, they are likely to aggregate and settle out before reaching the ocean.

Acknowledgments

We gratefully acknowledge financial support from the National Science Foundation (grant BES0731147), the Environmental Protection Agency (grant RD-83385701-0) and the Institute for Nanobiotechnology at Johns Hopkins University. We also acknowledge the use of the surface analysis laboratory at Johns Hopkins University. We thank Dennis Penisson for the construction of the custom titration vessel.

Supporting Information Available

Experimental details to determine the electrophoretic mobility, surface charge, and length distribution of O-MWCNTs; control studies to determine the influence of acetate buffer on the colloidal stability of O-MWCNTs (Figure S1); high- and low-resolution XP spectra for pristine and oxidized MWCNTs (Figure S2); distribution of oxygen functional groups on pristine and acid-treated multiwalled carbon nanotubes (Figure S3); analysis of the initial aggregation kinetics of O-MWCNTs (Figure S4); influence of pH on the colloidal stability of O-MWCNTs (Figure S5); pictorial representation of the influence of pH on the colloidal stability of O-MWCNTs (Figure S6); influence of electrolyte concentration on the electrophoretic mobility of O-MWCNTs, measured at pH 7 and 10 (Figure S7).This material is available free of charge via the Internet at http://pubs.acs.org.

Literature Cited

(1) Iijima, S. Helical microtubules of graphitic carbon. *Nature* **1991**, *354*, 56–58.

(2) Gibson, J. M.; Ebbensen, T. W.; Treacy, M. M. J. Exceptionally high Young's modulus observed for individual carbon nanotubes. *Nature* **1996**, *381*, 678–680.
(3) Ebbesen, T. W.; Lezec, H. J.; Hiura, H.; Bennett, J. W.; Ghaemi, H. F.; Thio, T. Electrical conductivity of individual carbon nanotubes. *Nature* **1996**, *382*, 54–56.
(4) Short, P.; McCoy, M. Companies Invest In Nanotubes. *Chem. Eng. News* **2007**, *85* (37), 20–21.
(5) Vaisman, L.; Marom, G.; Wagner, H. D. Dispersions of Surface-Modified Carbon Nanotubes in Water-Soluble and Water-Insoluble Polymers. *Adv. Funct. Mater.* **2006**, *16*, 357–363.
(6) Kwon, J.-Y.; Kim, H.-D. Preparation and Properties of Acid-Treated Multiwalled Carbon Nanotube/Waterborne Polyurethane Nanocomposites. *J. Appl. Polym. Sci.* **2005**, *96*, 595–604.
(7) Banerjee, S.; Wong, S. S. Rational Sidewall Functionalization and Purification of Single-Walled Carbon Nanotubes by Solution-Phase Ozonolysis. *J. Phys. Chem. B* **2002**, *106*, 12144–12151.
(8) Peng, Y.; Liu, H. Effects of Oxidation by Hydrogen Peroxide on the Structures of Multiwalled Carbon Nanotubes. *Ind. Eng. Chem. Res.* **2006**, *45*, 6483–6488.
(9) Rosca, I. D.; Watari, F.; Uo, M.; Akasaka, T. Oxidation of multiwalled carbon nanotubes by nitric acid. *Carbon* **2005**, *43*, 3124–3131.
(10) Li, X.; Niu, J.; Zhang, J.; Li, H.; Liu, Z. Labeling the Defects of Single-Walled Carbon Nanotubes Using Titanium Dioxide Nanoparticles. *J. Phys. Chem. B* **2003**, *107*, 2453–2458.
(11) Hiura, H.; Ebbesen, T. W.; Tanigaki, K. Opening and Purification of Carbon Nanotubes in High Yields. *Adv. Mater.* **1995**, *7*, 275–276.
(12) Li, Y.; Zhang, X.; Luo, J.; Huang, W.; Cheng, J.; Luo, Z.; Li, T.; Lui, F.; Xu, G.; Ke, X.; Li, L.; Geise, H. J. Purification of CVD Synthesized Single-wall Carbon Nanotubes by Different Acid Oxidation Treatments. *Nanotechnology* **2004**, *15*, 1645–1649.
(13) Martinez, M. T.; Callejas, M. A.; Benito, A. M.; Cochet, M.; Seeger, T.; Anson, A.; Schreiber, J.; Gordon, C.; Marhic, C.; Chauvet, O.; Maser, W. K. Modifications of Single-wall Carbon Nanotubes Upon Oxidative Purification Treatments. *Nanotechnology* **2003**, *14*, 691–695.
(14) Savage, T.; Bhattacharya, S.; Sadanadan, B.; Gaillard, J.; Tritt, T. M.; Sun, Y.-P.; Wu, Y.; Nayak, Y. W.; Car, R.; Marzari, N.; Ajayan, P. M.; Rao, A. M. Photoinduced oxidation of carbon nanotubes. *J. Phys. Condens. Matter* **2003**, *15*, 5915–5921.
(15) Fortner, J. D.; Kim, D.; Boyd, A. M.; Falkner, J. C.; Moran, S.; Colvin, V. L.; Hughes, J. B.; Kim, J.-H. Reaction of Water Stable C_{60} Aggregates with Ozone. *Environ. Sci. Technol.* **2007**, *41*, 7497–7502.
(16) Wiesner, M. R.; Lowry, G. V.; Alvarez, P.; Dionysiou, D.; Biswas, P. Assessing the Risks of Manufactured Nanomaterials. *Environ. Sci. Technol.* **2006**, *40*, 4336–4345.
(17) Dionysiou, D. D. Environmental Applications and Implications of Nanotechnology and Nanomaterials. *J. Environ. Eng.* **2004**, *130*, 723–724.
(18) Cho, H.-H.; Smith, B. A.; Wnuk, J.; Fairbrother, H.; Ball, W. P. Influence of Surface Oxides on the Adsorption of Naphthalene onto Multiwalled Carbon Nanotubes. *Environ. Sci. Technol.* **2008**, *42*, 2899–2905.
(19) Savage, N.; Diallo, M. S. Nanomaterials and Water Purification: Opportunities and Challenges. *J. Nanopart. Res.* **2005**, *7*, 331–342.
(20) Li, Y.-H.; Wang, S.; Luan, Z.; Ding, J.; Xu, C.; Wu, D. Adsorption of Cadmium(II) from Aqueous Solution by Surface Oxidized Carbon Nanotubes. *Carbon* **2003**, *41*, 1057–1062.
(21) Lubick, N. Risks of Nanotechnology Remain Uncertain. *Environ. Sci. Technol.* **2008**, *42*, 1821–1824.
(22) Owen, R.; Handy, R. Formulating the Problems for Environmental Risk Assessment of Nanomaterials. *Environ. Sci. Technol.* **2007**, *41*, 5582–5588.
(23) Chen, K. L.; Mylon, S. E.; Elimelech, M. Aggregation Kinetics of Alginate-Coated Hematite Nanoparticles in Monovalent and Divalent Electrolytes. *Environ. Sci. Technol.* **2006**, *40*, 1516–1523.
(24) Chen, K. L.; Elimelech, M. Influence of Humic Acid on the Aggregation Kinetics of Fullerene (C_{60}) Nanoparticles in Monovalent and Divalent Electrolyte Solutions. *J. Colloid Interface Sci.* **2007**, *309*, 126–134.
(25) Chen, K. L.; Elimelech, M. Aggregation and Deposition Kinetics of Fullerene (C_{60}) Nanoparticles. *Langmuir* **2006**, *22*, 10994–11001.
(26) Chen, K. L.; Mylon, S. E.; Elimelech, M. Enhanced Aggregation of Alginate-Coated Iron Oxide (Hematite) Nanoparticles in the Presence of Calcium, Strontium, and Barium Cations. *Langmuir* **2007**, *23*, 5920–5928.
(27) Mylon, S. E.; Chen, K. L.; Elimelech, M. Influence of Natural Organic Matter and Ionic Composition on the Kinetics and Structure of Hematite Colloid Aggregation: Implications to Iron Depletion in Estuaries. *Langmuir* **2004**, *20*, 9000–9006.
(28) He, Y. T.; Wan, J.; Tokunaga, T. Kinetic Stability of Hematite Nanoparticles: The Effect of Particle Sizes. *J. Nanopart. Res.* **2008**, *10*, 321–332.
(29) Phenrat, T.; Saleh, N.; Sirk, K.; Tilton, R. D.; Lowry, G. V. Aggregation and Sedimentation of Aqueous Nanoscale Zerovalent Iron Dispersions. *Environ. Sci. Technol.* **2007**, *41*, 284–290.
(30) Derjaguin, B. V.; Landau, L. Theory of the Stability of Strongly Charged Lyophobic Sols and of the Adhesion of Strongly Charged Particles in Solutions of Electrolytes. *Acta Physicochimica* **1941**, *14*, 633–662.
(31) Verwey, E. J.; Overbeek, J. T. G. *Theory of the Stability of Lyophobic Colloids*; Elsevier: New York, 1948.
(32) Chen, Q.; Saltiel, C.; Manickavasagam, S.; Schadler, L. S.; Siegel, R. W.; Yang, H. Aggregation Behavior of Single-Walled Carbon Nanotubes in Dilute Aqueous Suspension. *J. Colloid Interface Sci.* **2004**, *280*, 91–97.
(33) Shieh, Y.-T.; Liu, G.-L.; Wu, H.-H.; Lee, C.-C. Effects of Polarity and pH on the Solubility of Acid-treated Carbon Nanotubes in Different Media. *Carbon* **2007**, *43*, 1880–1890.
(34) Osswald, S.; Havel, M.; Gogotsi, Y. Monitoring Oxidation of Multiwalled Carbon Nanotubes by Raman Spectroscopy. *J. Raman Spectrosc.* **2007**, *38*, 728–736.
(35) Sano, M.; Okamura, J.; Shinkai, S. Colloidal Nature of Single-Walled Carbon Nanotubes in Electrolyte Solution: The Schulze-Hardy Rule. *Langmuir* **2001**, *17*, 7172–7173.
(36) Giordano, A. N.; Chaturvedi, H.; Poler, J. C. Critical Coagulation Concentrations for Carbon Nanotubes in Nonaqueous Solvent. *J. Phys. Chem. C* **2007**, *111*, 11583–11589.
(37) Zhang, X.; Sreekumar, T. V.; Liu, T.; Kumar, S. Properties and Structure of Nitric Acid Oxidized Single Wall Carbon Nanotube Films. *J. Phys. Chem. B* **2004**, *108*, 16435–16440.
(38) Cientifica. Nanotubes; 2004; http:// www.cientifica.com/www/summarys/Nanotubes_2004_ExSum.pdf.
(39) Langley, L. A.; Fairbrother, D. H. Effect of Wet Chemical Treatments on the Distribution of Surface Oxides on Carbonaceous Materials. *Carbon* **2007**, *45*, 47–54.
(40) Langley, L. A.; Villanueva, D. E.; Fairbrother, D. H. Quantification of surface oxides on carbonaceous materials. *Chem. Mater.* **2006**, *18*, 169–178.
(41) Li, Z. F.; Luo, G. H.; Zhou, W. P.; Wei, F.; Xiang, R.; Liu, Y. P. The Quantitative Characterization of the Concentration and Dispersion of Multi-walled Carbon Nanotubes in Suspension by Spectrophotometry. *Nanotechnology* **2006**, *17*, 3692–3698.
(42) Holthoff, H.; Egelhaaf, S. U.; Borkovec, M.; Schurtenberger, P.; Sticher, H. Coagulation Rate Measurements of Colloidal Particles by Simultaneous Static and Dynamic Light Scattering. *Langmuir* **1996**, *12*, 5541–5549.
(43) Gorham, J.; Wnuk, J.; Shin, M.; Fairbrother, D. H. Adsorption of Natural Organic Matter onto Carbonaceous Surfaces: an Atomic Force Microscopy Study. *Environ. Sci. Technol.* **2007**, *41*, 1238–1244.
(44) Hennrich, F.; Krupke, R.; Arnold, K.; Rojas Stuetz, J. A.; Lebedkin, S.; Koch, T.; Schimmel, T.; Kappes, M. M. The Mechanism of Cavitation-Induced Scission of Single-Walled Carbon Nanotubes. *J. Phys. Chem. B* **2007**, *111*, 1932–1937.
(45) Grolimund, D.; Elimelech, M.; Borkovec, M. Aggregation and Deposition Kinetics of Mobile Colloidal Particles in Natural Porous Media. *Colloids Surf. A* **2001**, *191*, 179–188.
(46) Hsu, J. P.; Kuo, Y. C. The Critical Coagulation Concentration of Counterions: Spherical Particles in Assymetric Electrolyte Solutions. *J. Colloid Interface Sci.* **1997**, *185*, 530–537.
(47) Fazli, H.; Golestanian, R. Aggregation Kinetics of Stiff Polyelectrolytes in the Presence of Multivalent Salt. *Phys. Rev. E* **2007**, *76*, 041801–041806.
(48) Brunner, R.; Gall, S.; Wilke, W.; Zrinyi, M. A Dynamic Light Scattering Study on Aggregation of Rodlike Colloidal Particles. *Physica A* **1997**, *239*, 477–485.
(49) Brunner, R.; Gall, S.; Wilke, W.; Zrinyi, M. Formation of Fractal Structures by Aggregation of Anisometric Iron(III)Hydroxide Particles. *Physica A* **1995**, *214*, 153–161.
(50) Esumi, K.; Ishigami, M.; Nakajima, A.; Sawada, K.; Honda, H. Chemical Treatment of Carbon Nanotubes. *Carbon* **1996**, *34*, 279–281.

(51) Hu, H.; Yu, A.; Kim, E.; Zhao, B.; Itkis, M. E.; Bekyarova, E.; Haddon, R. C. Influence of the Zeta Potential on the Dispersability and Purification of Single-Walled Carbon Nanotubes. *J. Phys. Chem. B* **2005**, *109*, 11520–11524.
(52) Bjelopavlic, M.; Newcombe, G.; Hayes, R. Adsorption of NOM onto Activated Carbon: Effect of Surface Charge, Ionic Strength, and Pore Volume Distribution. *J. Colloid Interface Sci.* **1999**, *210*, 271–280.
(53) Boehm, H. P. Surface oxides on carbon and their analysis: a critical assessment. *Carbon* **2002**, *40*, 145–149.
(54) Fuente, E.; Menendez, J. A.; Suarez, D.; Montes-Moran, A. Basic Surface Oxides on Carbon Materials: A Global View. *Langmuir* **2003**, *19*, 3505–3511.
(55) Yates, D. E.; Levine, S.; Helay, T. W. Site-binding Model of the Electrical Double Layer at the Oxide/Water Interface. *J. Chem. Soc. Faraday* **1974**, *70*, 1807–1818.

ES802011E